Fabrication and evaluation of a wide-band multilayer laminar-type holographic grating for use with a soft X-ray flat field spectrograph in the region of 1.7 keV

T. Imazono,[1] M. Ishino,[1] M. Koike,[1] H. Sasai,[2] and K. Sano[3]

Abstract

A multilayer laminar-type holographic grating having an average groove density of 2400 lines/mm is designed and fabricated for use with a soft X-ray flat field spectrograph covering the 1.7-keV region. A varied-line-spaced grooves pattern is generated by the use of an aspheric wavefront recording system and laminar-type grooves are formed by a reactive ion-etching method. Mo/SiO_2 multilayers optimized for the emission lines of Hf-M, Si-K, and W-M are deposited on one of the three designated areas on the grating surface in tandem. The measured first-order diffraction efficiencies at the respective centers of the areas are 18~20%. The flat field spectrograph equipped with the grating indicates a spectral line width of 8~14 eV for the soft x-ray emission spectra generated from electron-impact X-ray sources.

1. Introduction

Soft-X-ray flat-field grazing spectrographs have been convenient and successfully used for plasma diagnostics,[1] determination of the partial density of state of the valence band,[2, 3] in material sciences, monitoring the lasing conditions of soft X-ray lasers,[4] and more. The spectrograph consists solely of a concave grating and offers a high throughput taking advantage of the simplest configuration among the various soft X-ray spectrographs. The grating constant should be varied significantly to realize the quasi-straight focal curve required for plane imaging detectors like charged coupled detectors (CCDs). Such a grating is referred to as a varied-line-spacing (VLS) grating. Fabrication techniques for the soft-X-ray flat-field VLS gratings have been intensely investigated based on both mechanical ruling[1, 5] and holographic methods.[6, 7] We previously designed and fabricated a laminar-type holographic grating having a groove density of 2400 lines/mm for use with a soft X-ray flat field spectrograph covering the 0.7-6 nm region.[7].

---

[1] *Quantum Beam Science Directorate, Japan Atomic Energy Agency, 8-1 Umemidai, Kizugawa, Kyoto 619-0215, Japan*

[2] *Shimadzu Corp., 1-1 Nishinokyo-kuwabaracho, Nakagyo-ku, Kyoto 604-8511, Japan*

[3] *Shimadzu Emit Co. Ltd., 2-5-23 Kitahama, Chuo-ku, Osaka 541-0041, Japan*

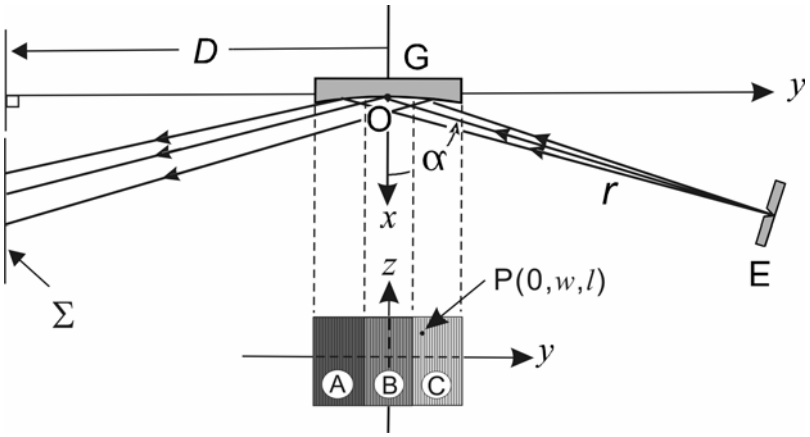

Fig. 1. Schematic diagram of the flat field spectrograph.

The varied-line-spaced grating pattern was generated by the use of an aspheric wavefront recording system and laminar–type grooves were formed by a reactive ion-etching method. The experimental results showed that the holographic grating indicated higher diffraction efficiency in <1.0 nm region and lower level higher order light over the whole wavelength range than a replica grating made from a mechanically ruled VLS grating. In addition, the spectral resolution and maximum first-order diffraction efficiency (>2%) at ~2 nm were comparable with the replica grating. The increasing demands for research relevant to inner-shell excitations based on soft X-ray emission and fluorescence spectroscopy in the energy region of a few keV have encouraged innovation in spectrographs to operate in this energy range. To extend the photon energy to the higher energy region it is necessary (1) to obtain new coating materials having a higher reflectivity due to the low reflectivities of conventional bulk materials like Au and Pt or (2) to use an extreme grazing incidence condition (> 89°). The latter option was evaluated experimentally by the use of a plane grating having a groove density of 600 lines/mm by use of a synchrotron radiation beam. The experiments revealed diffraction efficiencies of 3~6% in the 3~8 keV region.[8] However, this option is not valid for measurements of conventional dispersive sources due to its extremely narrow acceptance angle.

Recently we have fabricated a multilayer plane grating having a groove density of 1200 lines/mm depositing Co/SiO_2 and W/C multilayer coatings on the surface of laminar-type holographic master gratings.[9] The peak diffraction efficiencies of the Co/SiO_2 and W/C multilayer gratings were evaluated to be 47% at 6.0 keV and 38% at 8.0 keV, respectively. These should be attributed to the low overall surface roughness ≤ 1nm root-mean-square (rms), shallow laminar-type grooves having a depth of 3~4 nm suppressing the zero-th and higher order lights, and the Co/SiO_2 multilayer, which has high reflectivity in the 3~7 keV region.

In this paper, we describe the design of multilayer flat-field VLS gratings, evaluate their diffraction efficiency when the surface roughness and period length errors of the multilayers are present in the grating, compare the simulated performance with experimental results obtained at a synchrotron radiation facility, and show the results of the evaluation of the

spectral resolution by the use of the emission bands measured by use of electron-impact type x-ray tubes in the 1.7 keV region.

2. Grating design

A schematic diagram of the soft X-ray flat field spectrograph is shown in Fig. 1. A spherical grating G accepts light emerging through an entrance slit E. Diffracted light is focused on an image plane Σ that is parallel to the grating normal at its center. The mounting parameters are identical with a standard soft X-ray flat-field spectrograph[5] and expressed as follows: The distance from entrance slit E to the grating center O, r = 237.0 mm; incidence angle α = 87.0°; distance from the image plane perpendicular to the y-axis to the grating center D = −235 mm. Therefore, the distance from grating center to the image plane is r' = 235/cos(π/2 + β_0), where β_0 is the diffraction angle of the principal diffracted ray.

We chose a photon energy range of 1.6~1.8 keV to cover three emission lines of Hf-M$_\alpha$ (1644.6 eV), Si-K$_\alpha$ (1740.0 eV), and W-M$_\alpha$ (1775.4 eV). The basic design parameters are as follows: the radius of curvature of the grating R = 4833 mm; effective grating constant σ = 1/2400 mm; the spectral order m = +1; ruled width W = 46 mm; ruled height L = 26 mm; wavelength of the recording laser λ_0 = 441.6 nm.

We used a combination of an aspheric wavefront resulting from the reflection of a spherical wavefront from a spherical mirror and a spherical wavefront to record a VLS holographic grating.[10]

The groove number n is expressed by a power series of the coordinates P(0,w,l) on the nth grooves as

$$n\sigma = w + \Gamma\left[0.5\left(n_{20}w^2 + n_{02}l^2 + n_{30}w^3 + n_{12}wl^2\right) + 0.125(n_{40}w^4 + 2n_{22}w^2l^2 + n_{04}l^4) + \cdots\right] \qquad (1)$$

where $\Gamma = \sigma/\lambda_0$. The explicit expressions of the groove parameters n_{ij} for the holographic grating recorded with aspheric wavefront recording optics are given in [10]. The following

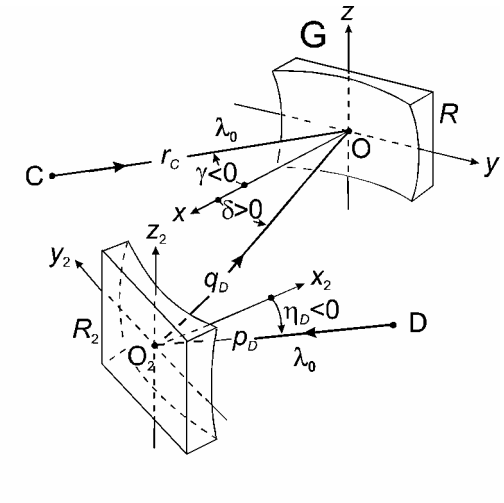

Fig. 2. Schematic diagram of the recording system composed of a combination of an aspheric wavefront and aspheric wavefront to record a VLS holographic grating.

recording parameters were determined by means of an analytical design method:[10, 11]: distance CO r_C = 554.0 mm, radius of curvature of M_2R_2 = 400.0 mm, distance DO_2 p_D = 1073.0 mm, distance O_2O q_C = 250.0 mm, angle of $\angle COx$ $\gamma = -50.80°$, angle of $\angle O_2Ox$ $\delta = 16.55°$, angle of $\angle DO_2x_2$ $\eta_D = 55.93°$. For the definition of the parameters refer to Fig. 2. This holographic recording system provides for he grating the groove parameter values of Γn_{20} = -6.198 × 10^{-3} mm^{-1}, Γn_{02} = 5.078 × 10^{-3} mm^{-1}, Γn_{30} = 2.274 × 10^{-5} mm^{-2}, Γn_{12} = -3.939 × 10^{-5} mm^{-2}, Γn_{40} = -5.860 × 10^{-7} mm^{-3}, Γn_{22} = 3.974 × 10^{-7} mm^{-3}, and Γn_{04} = -1.637× 10^{-7} mm^{-3}.

The theoretical resolution of the standard spectrograph equipped with the holographic gratings thus designed was evaluated by means of ray tracing. We assumed in performing ray tracing that the entrance slit was a self-luminous source having dimensions of 1 μm×1 μm and both the gratings had a ruled area of 46 mm (W)×26 mm (H). The length of the astigmatic images corresponding to the grating height of 26 mm is ~60 mm. This is too long to be accepted by normal detectors. Therefore we assumed a vertical aperture having a 10-mm height in front of the image plane. Figure 3 shows the spot diagrams and line profiles constructed with 500 rays for three wavelengths of λ and $\lambda \pm \lambda/200$ (λ = 0.698, 0.713, and 0.754 nm). The line profiles were constructed by counting the number of spots falling into individual zones of 4-μm width in the respective spot diagrams. In each diagram the value of λ, the position on the x-axis of the spot formed by the principal ray, the standard deviation σ_λ of the spectral spread for the rays of λ and the resolving power $\Re$ are given. Here, σ_λ is defined as the product of the standard deviation σ_X of the distribution of ray-traced spots in the x-direction and the reciprocal linear dispersion at λ. The resolving power $\Re$ calculated for Fig. 3(a)-3(c) are 1005, 1136, and 913, respectively. The pixel size of the commercial CCD detectors which are frequently used for these kind of spectrographs is 13~20 μm and the

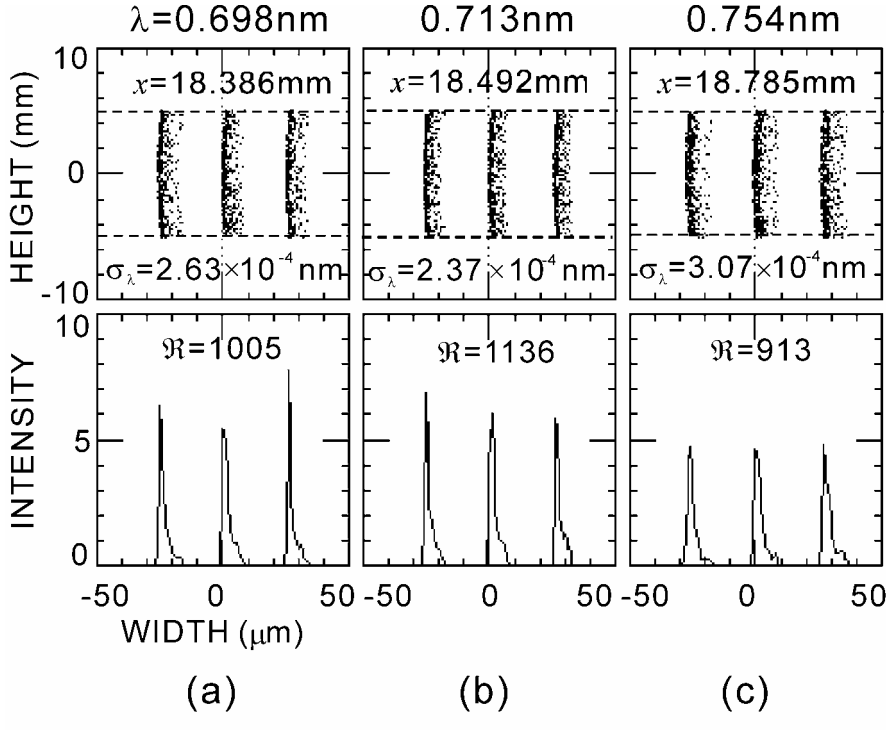

Fig. 3. Spot diagrams and line profiles.

corresponding resolving power is 200~300. Therefore, it is concluded that the aberration of the grating thus designed would not affect the practical spectral resolution.

3. Multilayers design

As the result of theoretical feasibility study we choose Mo and SiO_2 as the material pair for the multilayer because better reflectivity is attained than the previous Co/SiO_2 pair[9] in the 1.6~1.8 keV region. It is considered to the smaller extinction coefficient of Mo than that of Co between Co-M and Mo-L absorption edges (0.78-2.5 keV). The detail experimental comparison on the reflectivities of Mo/SiO_2 and Co/SiO_2 multilayers and their thermal stabilities will be published elsewhere.

When the plane grating is illuminated with quasi-parallel light, the multilayer period can be simply determined by the generalized Bragg condition based on kinematical theory.[12] However, for the current spectrograph the spherical grating has a radius of curvature on the surface and the grating is illuminated by the divergent light from the entrance slit (or point source) located at a finite distance. Therefore the local incidence angle varies depending on the respective incident points on the grating surface. Furthermore the multilayer coating is to enhance the diffraction efficiency of light having three discrete photon energies (or wavelengths), i.e., Hf-M, Si-K, and W-M lines. To compromise these requirements we split the grating surface of 48 mm (W) × 26 mm (H) into three areas "A", "B", and "C" in the *y*-direction (refer to Fig. 1). In the each area we optimized the multilayer period, MP, for one of the three-photon energies assuming the local incident angle and the local slant angle of the grating surface for the following three cases:

Case I: All areas are coated with a multilayer period optimized for Si-K_α line;

Case II: Areas A, B, and C are coated with multilayer periods optimized for W-M_α, Si-K_α, and Hf-M_α lines, respectively;

Case III: Areas A, B, and C are coated with multilayer periods optimized for Hf-M_α, Si-K_α, and W-M_α lines, respectively.

In the calculation we assumed the groove depth and duty ratio of the groove (ledge/grating period) were 3 nm and 0.4, respectively to suppress the zeroth-order and maximize first-order efficiencies.[9] Also the number of material pairs of the multilayer and ratio of (Mo thickness)/(periodic length) were chosen as 30 and 0.4, respectively. The values of the obtained MPs are shown in Table I.

Table I. Relation between the coating areas A, B, and C and the multilayer periods MP. The MPs were optimized for the respective spectral lines, SP, and the local incident angles at the center of the areas shown in the table.

	Case I		Case II		Case III	
Area	SP	MP (nm)	SP	MP (nm)	SP	MP (nm)
A			W-M_α	5.66	Hf-M_α	6.11
B	Si-K_α	5.89	Si-K_α	5.89	Si-K_α	5.89
C			Hf-M_α	6.31	W-M_α	5.83

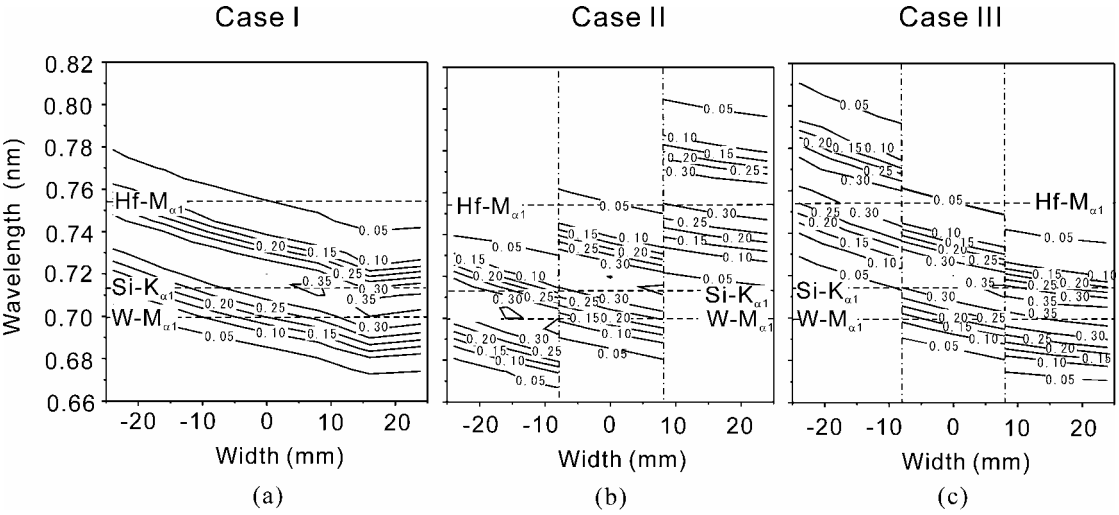

Fig. 4. Diffraction efficiencies calculated for incident wavelengths (ordinate) and incident points on the grating in *y*-direction (abscissa) for Cases I (a), II (b), and III (c).

Figure 4 shows the calculated diffraction efficiencies vs. incident point and incident wavelength for the first order ($m = +1$) for Cases I (a), II (b), and III (c) by use of a simulation code based on coupled wave and modal theories.[13] The indices of refraction derived from the atomic scattering factors were used.[14] The ordinate and abscissa refer to the incident wavelengths and *y*-coordinate of the incident points on the grating, respectively. The calculation was made taking into account the local grating constant, local incident angle, and slant angle of the grating surface due to the curvature of the grating blank. It is easily found that the diffraction efficiency distribution is not sufficient to cover the hafnium M_α (0.754 nm) spectrum in Case I. On the other hand the efficiency peak is located in the designated area for the respective wavelengths in Cases II and III.

To illustrate the diffraction efficiencies for the three emission lines more clearly the diffraction efficiencies at their wavelengths (the cross section views at dashed lines) are

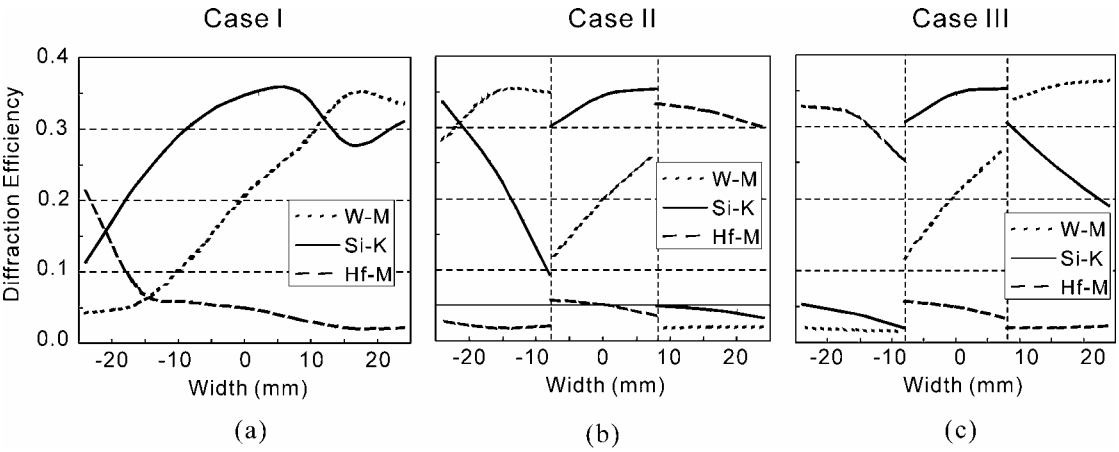

Fig. 5.Calculated diffraction efficiencies vs. incident points in the *y*-direction on the grating calculated for the design spectral lines for Cases I (a), II (b), and III (c).

shown in Fig.5. The figures (a), (b), and (c) correspond to Cases I, II, and III, respectively.

The diffraction efficiency for the Hf-M_α of Case I is significantly inferior to those of Cases II and III. In Cases II and III the diffraction efficiency of each emission line exceeds 30% in the area where the multilayer coating is optimized for the respective wavelengths. Finally, we chose Case III for the multilayer coating scheme because of the relatively smooth transition of the diffraction efficiencies at the borders of the coating areas.

4. Fabrication of the grating

The laminar grating was fabricated at Shimadzu Corporation, Kyoto. The substrate of the master holographic grating was synthetic quartz with an rms roughness of 0.3 nm as measured by an interference microscope with a 50x objective. Use was made of the recording system shown in Fig.2. The sinusoidal grooves pattern in the developed photoresist was used as an etching mask. The sinusoidal grooves of the holographic grating thus recorded were processed into laminar grooves by reactive ion beam etching in CHF_3.[15] The groove depth and duty ratio (ratio of land-width to period) were 3 nm and 0.46, respectively, as measured by a stylus surface profiler.

The Mo/SiO_2 multilayers were coated on the laminar grating at the Japan Atomic Energy Agency, Kyoto, Japan by the ion beam sputtering method. The multilayer period lengths were intended to be values shown in Case III, Table I. The number of periods and ratio of (Mo thickness)/(periodic length) were chosen to be 30 periods and 0.4, respectively. The resultant multilayer periods for the three areas were measured by an X-ray diffractometer at 0.154 nm (Cu-K_α). The results obtained were 6.12 ± 0.01 nm (6.11 nm), 5.88 ± 0.05 nm (5.89 nm), and 5.87 ± 0.07 nm (5.83 nm) for areas A, B, and C, respectively. The designed period lengths are shown in the parentheses for reference. Comparing the measured and designed multilayer periods the error is less than 2%.

5. Evaluation of the grating

The diffraction efficiency of the multilayer grating was measured at the evaluation beamline[16, 17] for soft X-ray optical elements at BL-11 of the SR Center, Ritsumeikan University. The measurements were performed for the three areas at various incident angles. The purposes of the measurement are twofold. One is to measure the absolute diffraction

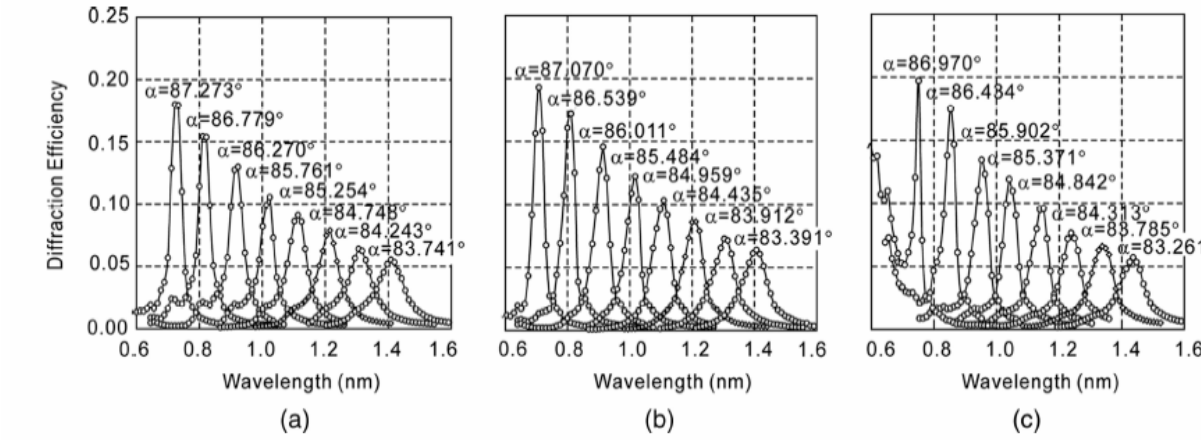

Fig. 6. The measured absolute efficiency for the various incident angles, α for areas A (a), B (b), and C (c).

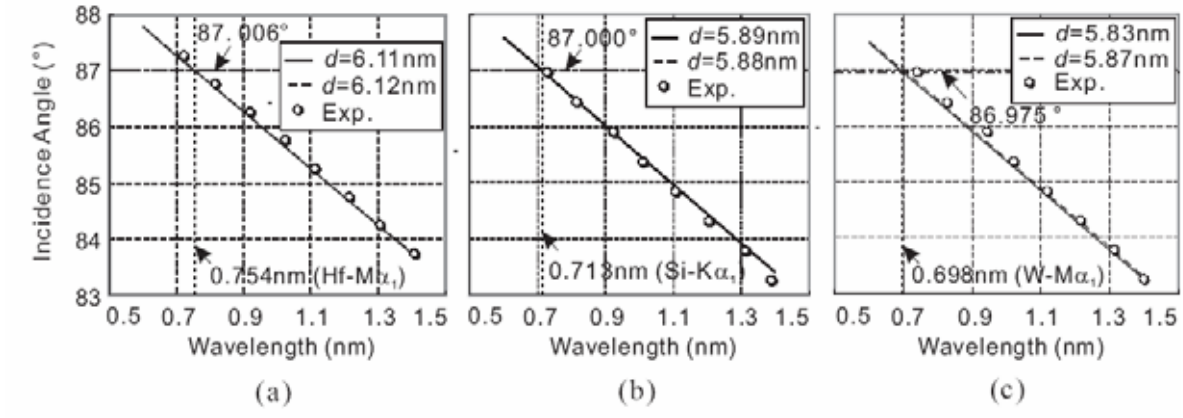

Fig. 7. Efficiency maxima calculated assuming the design multilayer periods (full lines) and those calculated assuming the multilayer periods measured by the X-ray diffractometer (dashed lines) as functions of the wavelengths and incidence angles as well as the measured efficiency maxima (open circles) for the areas A (a) , B (b), and C (c). The design wavelengths and local incidence angles at the centers of the respective areas are indicated with dotted lines.

efficiency for each area. The other is to check the matching among the local incidence angle, local grating constant, and the efficiency maximum of the multilayer for each area.

Figure 6 shows the absolute diffraction efficiencies for the first order (m = +1) measured at the centers of the areas A (a), B (b), and C (c). The incidence angles shown for the respective curves were those measured from the normals at the centers of the respective areas. The relation between the incidence angles and efficiency maxima obtained theoretically and experimentally should be examined carefully to check the coincidence with the design and resultant characters of the multilayers.

Figure 7 is the diagram showing the measured efficiency maxima (open circles) with the wavelengths and incidence angles for the areas A (a), B (b), and C (c). The efficiency maxima calculated assuming the design multilayer periods (full lines) and those calculated assuming the multilayer periods measured by the X-ray diffractometer (dashed lines) are also shown. The design wavelengths and local incidence angles at the centers of the respective areas are indicated with dotted lines. Therefore the vicinity of the cross point of two dotted lines is the valid area for the measurements of the respective emission lines. Exploiting and interpolating the lines connecting the measured efficiency maxima it was found that the discrepancies of the wavelengths were +0.019 nm, +0.012 nm, and +0.027 nm from the design wavelengths in areas A, B, and C, respectively, and smaller than the full width at half maximum (FWHM) of ~0.04 nm of the efficiency curves at ~0.7 nm (refer to Fig. 6).

Figure 8 shows the measured and calculated efficiencies. The black squares and solid curves show the measured and calculated diffraction efficiencies for m = 0 and +1,[13, 14] respectively. The multilayer period lengths were assumed to be the values evaluated by the x-ray diffractometer.

The difference between the measured and calculated efficiency could be attributed to the surface roughness at the top and at the boundaries inside the multilayer. In addition, several thin diffused layers such as molybdenum silicide might have formed at the interfaces.[18] To estimate the magnitude of these effects we applied the Debye-Waller factor,[19]

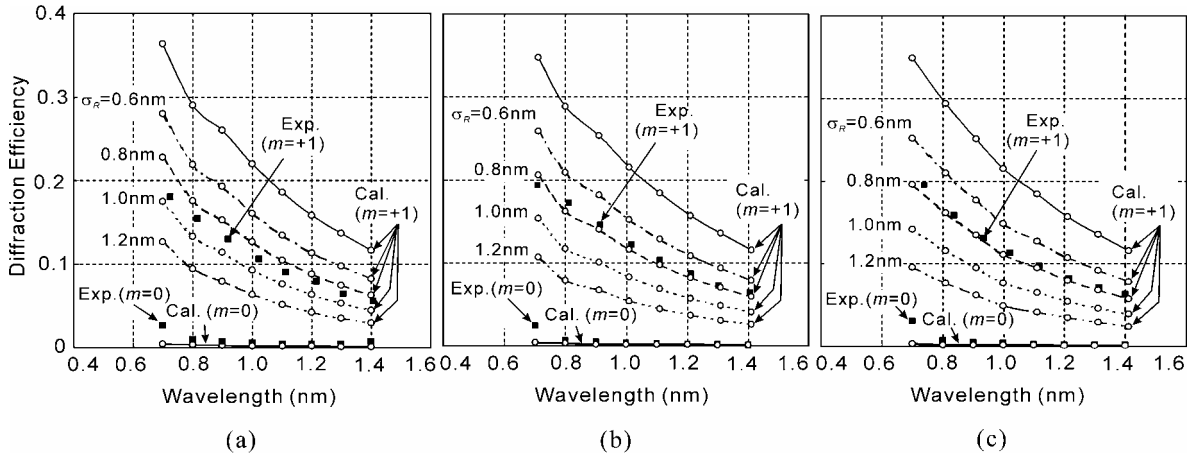

Fig. 8. The measured and calculated efficiency curves for the zeroth and first diffraction orders (m = 0, +1). The black square symbols and solid lines show the measured and calculated diffraction efficiencies, respectively. The broken lines indicate the calculated diffraction efficiencies with Debye-Waller factors of 0.6, 0.8, 1.0, and 1.2 nm rms.

$$E = E_0 \exp\left[-\left(4\pi\sigma_R \cos\alpha / \lambda\right)^2\right], \qquad (2)$$

to the calculated diffraction efficiencies for m = +1, where E_0 is the calculated diffraction efficiency of a multilayer and σ_R is the rms roughness of the interfaces in the multilayer. The efficiencies calculated for σ_R = 0.6, 0.8, 1.0, and 1.2 nm are indicated by the broken curves.

The comparison of the measured and calculated efficiencies for m = +1 suggests that the multilayer grating has an rms roughness of 0.7~0.9 nm. It is noted that the roughness is smaller than the ~1.0 nm of our previous gratings having a groove density of 1200 lines/mm[9] even though its groove density, 2400 lines/mm, is two times higher. Also the zeroth order efficiencies are well suppressed. It is attributed to the appropriate design and fabrication of the groove structure and resultant small roughness of the grooves and multilayer structures.

A measurement of the spectral resolution was performed using a spectrograph with a laboratory X-ray source. This system consists of a soft X-ray source (McPherson Model 642), a vacuum spectrograph having the mounting parameters as described in Sec. 2., an entrance slit of 25 μm (W) × 10 mm (H), and a back-illuminated CCD detector having an imaging array (pixels) of 1340 × 400 and pixel size of 20 μm × 20 μm (Princeton Instruments PI-SX 400 (B)). The standard bulk materials of Hf, Si, and W were used as the target anodes of the soft X-ray source.

Figure 9 shows the emission bands of Hf-M, Si-K, and W-M generated at the high voltage powers of 5 kV/0.48 mA, 5 kV/0.04 mA, and 5 keV/0.2 mA, respectively. The respective spectra were normalized by the peak intensities of Hf-M_α, Si-K_α, and W-M_α. The FWHMs of the line profiles of Hf-M_α, Si-K_α, and W-M_α are 13.7 eV, 8.0 eV, and 8.7 eV, respectively. Considering the spectral dispersion of 42 eV/mm in the image plane the spectral-band-widths corresponding to the slit width of 25 μm and the pixel size of 20 μm are 10.4 eV and 8.3 eV, respectively. Therefore this denotes that the measured spectral resolution is close to the instrumental limitation of the system used for this experiment.

To confirm the advantage in using the multilayer grating the emission band of Si-K was

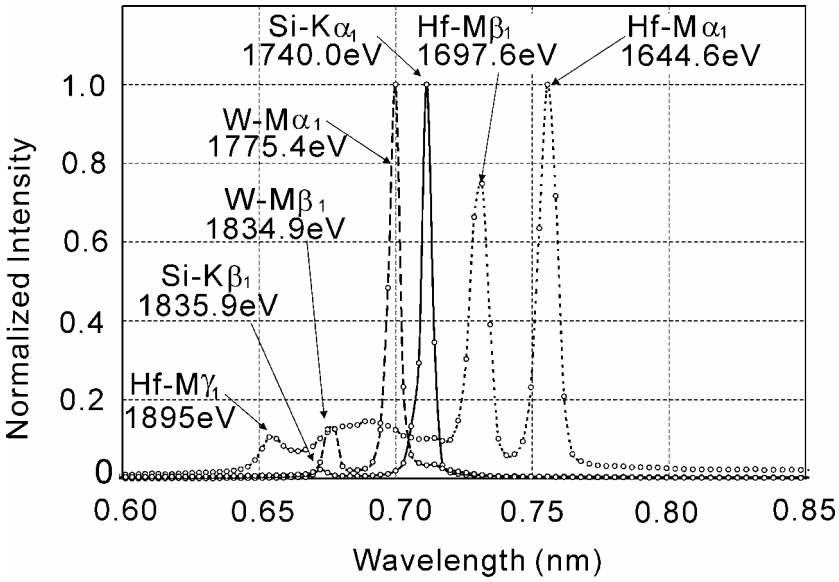

Fig. 9. The emission bands of Hf-M, Si-K, and W-M. The intensities of the respective spectra were normalized by the peak intensities of Hf-M_α, Si-K_α, and W-M_α.

also measured with a spectrograph equipped with an Au-coated VLS laminar-type grating.[7] The grating has the same effective groove density, 2400 lines/mm, as that of the multilayer grating, and the spectrograph has almost the same mounting conditions as those of the system described in Sec. 2 except for the incidence angle of 88.65°. When the source was operated at the high voltage power, 5 kV/0.04 mA, which was used for the multilayer grating no distinguishable signal was observed. Finally, at the high voltage power of 5 kV/0.60 mA, we observed a band at one forth of the intensity of the case with the multilayer grating. Even taking into account the nonlinearity occurring between the high voltage current and the amount of the incident flux we conclude that the throughput of the spectrograph employing the multilayer grating is estimated to be more than one order magnitude larger than that equipped with the Au-coated grating at the photon energy of the Si-K band.

6. Conclusion

A multilayer varied-line-spacing laminar-type grating having a nominal groove density of 2400 lines/mm and designed for working in the 1.7-keV region has been developed to use in a standard flat field spectrograph which is used for the <0.3 keV region keeping the same incidence angle of 87°. To extend the high diffraction efficiency for the energy region of over a 100 eV wide region a method was devised to deposit multilayers having multiple periods dividing the grating surface into three sub areas. The performance of the fabricated grating has been evaluated in terms of the diffraction efficiency and spectral resolution. The results show that the experimental diffraction efficiencies are ~50% of the theoretical efficiencies and the deterioration corresponds to a surface roughness of 0.7~0.9 nm rms. Regarding to the spectral resolution of the spectrograph equipped with the multilayer grating the FWHMs of the measured emission bands of Hf-M_α, Si-K_α, and W-M_α show 8.0~13.7 eV which are almost equivalent to those restricted by the slit width and pixel size of the detector.

Acknowledgement

A part of this research is conducted under the project titled “Development of an EELS/XES electron microscope for electronic structure analyses”, which is one of the leading projects of the Ministry of Education, Culture, Sports, Science and Technology, Japan.

References

[1] N. Nakano, H. Kuroda, T. Kita, and T. Harada, “Development of a flat-field grazing-incidence XUV spectrometer and its application in picosecond XUV spectroscopy,” Appl. Opt. **23**, 2386-2392 (1984).

[2] T. Imazono, Y. Hirayama, S. Ichikura, O. Kitakami, M. Yanagihara, and M. Watanabe, “Interdiffused layers in antiferromagnetically coupled Fe/Si multilayers studied by soft-X-ray fluorescence spectroscopy,” Jpn. J. Appl. Phys. **43**, 4334-4337 (2004).

[3] M. Terauchi and M. Kawana, “Soft-X-ray emission spectroscopy based on TEM -Toward a total electronic structure analysis-,” Ultramicroscopy **106** (11-12), 1069-1075 (2006).

[4] T. Kawachi, A. Sasaki, M. Tanaka, M. Kishimoto, N. Hasegawa, K. Nagashima, M. Koike, H. Daido, and Y. Kato, “Observation of strong soft-x-ray amplification at 8.8 nm in the transient collisional-excitation scheme,” Phys. Rev. **A 69**, 033805 (2004).

[5] T. Harada and T. Kita, “Mechanically ruled aberration-corrected concave grating,” Appl. Opt. **19**, 3987-3993, (1980).

[6] M. Koike, T. Namioka, E. Gullikson, Y. Haradad, S. Ishikawa, T. Imazono, S. Mrowka, N. Miyata, M. Yanagihara, J. H. Underwood, K. Sano, T. Ogiwara, O. Yoda, S. Nagai, “Varied-line-spacing laminar-type holographic grating for the standard soft X-ray flat-field spectrograph,” Proc. SPIE **4146**,163-170 (2000).

[7] M. Koike, K. Sano, E. Gullikson, Y. Harada, H. Kumata, “Performance of laminar-type holographic grating for a soft X-ray flat field spectrograph in the 0.7-6 nm region,” Rev. Sci. Instrum., **74**, 1156-1158 (2003).

[8] P. A. Heimann, M. Koike, and H. A. Padmore, “Dispersive x-ray absorption spectroscopy with gratings above 2 keV,” Rev. Sci. Instrum. **76**, 063102 (2005).

[9] M. Ishino, P. A. Heimann, H. Sasai, M. Hatakeyama, H. Takenaka, K. Sano, E. M. Gullikson, and M. Koike, “Multilayer laminar-type diffraction gratings achieving high diffraction efficiencies in the 1-8 keV region,” Appl. Opt., **45**, 6741-6745 (2006).

[10] T. Namioka and M. Koike, "Aspheric wavefront recording optics for holographic gratings," Appl. Opt., **34**, 2180-2186 (1995).

[11] M. Koike and T. Namioka, "A merit function for the design of grating instruments," Appl. Opt., **33**, 2048-2056 (1994).

[12] W. K. Warburton, “On the diffraction properties of multilayer coated plane gratings,” Nucl. Instrum. Methods Phys. Res. **A 291**, 278-285 (1990).

[13] GSOLVER V4.2c, Grating Solver Development Co., Allen, Texas.

[14] B. L. Henke, E. M. Gullikson, and J. C. Davis, “X-ray interactions: photoabsorption, scattering, transmission, and reflection at E = 50 – 30,000 eV, Z = 1 – 92,” At. Data Nucl. Data Tables **54**, 181-342 (1993).

[15] E. Ishiguro, K. Yamashita, H. Ohashi, M. Sakurai, O. Aita, M. Watanabe, K. Sano, M. Koeda, and T. Nagano,” Fabrication and characterization of reactive ion beam etched SiC gratings,” Rev. Sci. Instrum., **63**, 1439-1442 (1992).

[16] M. Koike, K. Sano, O. Yoda, Y. Harada, M. Ishino, N. Moriya, H. Sasai, H. Takenaka, E.

Gullikson, S. Mrowka, M. Jinno, Y. Ueno, J. H. Underwood, T. Namioka, “New evaluation beamline for soft X-ray optical elements,” Rev. Sci. Instrum. **73**, 1541-1544 (2002).

[17] M. Koike, K.Sano, Y. Harada, O. Yoda, M. Ishino, K. Tamura, K. Yamashita, N. Moriya, H. Sasai, M. Jinno, and T. Namioka, “New type of Monk-Gillieson monochromator capable of covering a 0.7-25 nm range,” Proc. SPIE **4782**, 300-307 (2002).

[18] T. B. Massalski, Binary Alloy Phase Diagrams (American Society for Metals, 1986).

[19] E. Spiller, Soft X-ray Optics (SPIE Press, Bellingham, WA, 1994), pp.111-114.